frontiers | Frontiers in Communications and Networks

ORIGINAL RESEARCH
published: 20 May 2022
doi: 10.3389/frcmn.2022.746201

# Mixed FSO/RF Based Multiple HAPs Assisted Multiuser Multiantenna Terrestrial Communication

*Praveen Kumar Singya* and Mohamed-Slim Alouini*

*Computer, Electrical, and Mathematical Science and Engineering (CEMSE) Division, King Abdullah University of Science and Technology (KAUST), Thuwal, Saudi Arabia*

In this work, a mixed free-space optics (FSO)/radio-frequency (RF) based multiple serial high altitude platforms (HAPs) assisted multiuser multiantenna terrestrial communication system is considered. For the considered multi-hop system, earth station to HAP and HAP to HAP links are assumed as FSO links, and HAP to terrestrial mobile users (MUs) link is assumed as RF link. At the FSO detector both the heterodyne detection and intensity modulation direct detection techniques are considered. Atmospheric turbulence of the ES to HAP FSO link is modeled with Gamma-Gamma fading along with the pointing error impairments. As HAP situates in the stratosphere, negligible atmospheric turbulence exists at HAP altitude (20 km), hence, only pointing error is considered for the inter HAP links. Further, the HAP consists of multiantenna array to provide high data-rates to the terrestrial users via RF links, considered to be Nakagami-m distributed. The intermediate HAPs perform selective decode-and-forward relaying and opportunistic user scheduling is performed for the best user selection. For the performance analysis, analytical expression of overall outage probability is obtained and the impact of various selection parameters like pointing error, FSO detection type, MU selection, number of antennas, and RF fading severity are observed on the outage performance. Asymptotic outage probability is also derived to obtain the diversity order of the considered communication system. Further, considering various modulation schemes, a generalized average bit-error-rate expression is derived and the impact of pointing error, FSO detection type, MU selection, number of antennas, and RF fading severity are observed on its performance. Finally, derived results are validated through Monte-Carlo simulations.

**Keywords: free-space optics, high altitude platform, gamma-gamma fading, pointing error, outage probability, average bit-error-rate**

OPEN ACCESS

***Edited by:***
*Steve Hranilovic,*
*McMaster University, Canada*

***Reviewed by:***
*Guanjun Xu,*
*East China Normal University, China*
*Milica Petkovic,*
*University of Novi Sad, Serbia*

****Correspondence:***
*Praveen Kumar Singya*
*praveen.singya@kaust.edu.sa*

***Specialty section:***
*This article was submitted to Optical Communications and Networks, a section of the journal Frontiers in Communications and Networks*

***Received:*** *23 July 2021*
***Accepted:*** *25 February 2022*
***Published:*** *20 May 2022*

***Citation:***
*Singya PK and Alouini M-S (2022) Mixed FSO/RF Based Multiple HAPs Assisted Multiuser Multiantenna Terrestrial Communication. Front. Comms. Net 3:746201. doi: 10.3389/frcmn.2022.746201*

## 1 INTRODUCTION

For reliable and robust high data-rate communication for various wireless applications including the emergency disastrous situations, temporary mass events, and even in military applications, promptly deployable flying base stations such as unmanned aerial vehicles (UAVs) have gained significant research attention as they are capable to provide high data-rates with improved capacity and coverage, targeted for beyond fifth generation (5G) communications(Zhan et al., 2011; Mozaffari et al., 2019). UAVs are broadly categorized into low altitude platform (LAP) and high altitude platform (HAP) based on their size and operating range. The LAPs are situated only few hundred meters above the earth surface, however, the HAPs are usually situated in stratosphere around

17–25 km (km) altitude from the earth surface. As the HAP situates in stratosphere, the wind velocity is low and atmospheric turbulence is negligible, hence, the HAP can be in quasi-static position and is capable to provide ubiquitous connectivity (Kurt et al., 2021). Due to the enhancement in communications technologies, lightweight composite materials, improved efficiency of solar panels and antenna, HAP became an viable aerial network component for various communication applications. The HAPs can be deployed easily and rapidly, their maintenance is easy, and having moderate operational cost than satellite which makes them economically feasible (Fidler et al., 2010; Kurt et al., 2021). Various technological trends of HAPs and their applications in wireless communications have been seen in (d'Oliveira et al., 2016). On the other hand, free-space optics (FSO) has been proven as an efficient replacement to radio-frequency (RF) due to its high operational bandwidth with improved capacity to fulfill the increasing demand of high data-rates for present and future wireless communication networks. FSO operates in unlicensed band, having low cost and easy deployment, and provides high-speed line-of-sight (LoS) communication (Singya et al., 2020; Trichili et al., 2020). The FSO links provide high data-rate secured transmission than the RF links, however requires LoS communication. Further, atmospheric turbulence and weather issues are more severe in terrestrial mobile communication which limits the FSO link's performance. In such situations, RF links provide more robust communication to mobile users (MUs) than the FSO links. Thus, a hybrid system which can utilize the high data-rate capability of FSO links and the reliable transmission through RF links to terrestrial MUs has gained significant research attention (Trichili et al., 2021).

Various HAP networks like HAPCOS and CAPANINA in Europe, Helicos in USA, SkyNet is Asia, etc. have been deployed successfully for broadband data transmission to a larger distance (in hundreds of km). A considerable work on HAP networks have been seen in the literature. In (Vaiopoulos et al., 2013), authors proposed a HAP assisted setup for WiMAX orthogonal frequency division multiplexing (OFDM) transmission and derived the outage probability. In (Fidler et al., 2010), authors have shown various field trials to and from HAP using optical links to provide high data-rates. In (David et al., 2004), various considerations for inter-HAP optical link design are shown. In (Parthasarathy et al., 2014), channel modeling of inter-HAP optical link is proposed. In (Shibata et al., 2020), a gigabit HAP system for mobile communications is proposed. An HAP assisted ground to satellite uplink FSO/RF system is proposed in (Swaminathan et al., 2021) with Gamma-Gamma and shadowed-Rician fading for FSO and RF links, respectively, and various performance measures are derived. In (Singya and Alouini, 2021), an HAP assisted downlink hybrid FSO/RF based multiuser multiantenna terrestrial communication system is proposed, where the FSO link is characterized with the Gamma-Gamma distribution with pointing error impairments and Nakagami-m distribution is preferred for RF links. For the performance analysis, analytical expressions of outage probability, asymptotic outage probability, ergodic capacity, effective capacity, and generalized average symbol-error-rate (ASER) expressions of hexagonal-quadrature amplitude modulation (QAM), cross-QAM, and rectangular QAM are derived. (Liu et al., 2020) focuses on amplify-and-forward (AF) based HAP assisted satellite-terrestrial communication with Gamma-Gamma and Rayleigh distributions for the FSO and RF links, respectively, and obtained the outage probability. In (Antonini et al., 2006), capacity and efficiency of FSO link between the satellite and HAP are obtained for its feasibility. In (Gao et al., 2021), optimization of an intelligent reconfigurable surface assisted HAP network is proposed for downlink communication to terrestrial MUs.

However, a significant work is witnessed on various hybrid FSO/RF systems in the literature. (Bhatnagar and Arti, 2013) considers a hybrid RF/FSO based satellite-terrestrial communication system, where Gamma-Gamma and shadowed-Rician distributions are considered for the FSO and RF links, respectively. Further, analytical ASER expression for M-ary phase-shift keying (MPSK) and asymptotic results are obtained. (Zedini et al., 2016) focuses on a hybrid FSO/RF system with Nakagami-m and Gamma-Gamma fading for the RF and FSO links, respectively, and the analytical expressions of ergodic capacity, outage probability, and bit-error-rate (BER) of binary phase-shift keying (BPSK) are derived. (Chen et al., 2019) covers energy harvesting in hybrid FSO/RF system by obtaining the outage probability. An FSO/RF based satellite-terrestrial communication system is considered in (Ahmad et al., 2017), where satellite is connected through the optical feeder link and provides RF connectivity to terrestrial users, and various performance measures are derived for analysis. (Zedini et al., 2020) focuses on an FSO/RF based satellite-terrestrial communication system with Gamma-Gamma distributed uplink optical feeder link and shadowed-Rician distributed downlink RF terrestrial users links, and ergodic capacity, outage probability, and BER expressions of BPSK are derived. In (Sharma et al., 2019), switching-based FSO/RF system is proposed and various performance measures are obtained. (Lee et al., 2020) focuses on the data throughput maximization for UAV based FSO/RF system. Further, in (Singya et al., 2020), ASER performance of various higher order complex QAM schemes is obtained for a mixed RF/FSO system with outdated channel state information. In (Xu and Song, 2021) and (Xu and Song, 2020), hybrid RF/FSO based communication systems are considered, where RF link is characterized with $\kappa - \mu$ distribution and the FSO link is characterized with the $\mathcal{M}$- distribution with pointing error impairments. For performance analysis, outage probability, asymptotic outage probability, ergodic capacity, and ABER results are obtained. In (Xu and Zhang, 2021), a hybrid RF/FSO based deep space communication system is considered, where exponentiated Weibull and Nakagami-m distributions are considered respectively for the FSO and RF links; and outage probability, ergodic capacity, and ABER of MPSK are derived.

In the literature, some papers have discussed FSO based multi-hop communication systems. In (Datsikas et al., 2010; Zedini and Alouini, 2015; Ashrafzadeh et al., 2020), authors have analyzed the performance of multi-hop FSO systems. (Altubaishi and Alhamawi, 2019) focuses on the capacity analysis of a multi-

**TABLE 1 |** Various related works.

| Communication systems | References | Channel models | Practical considerations | Performance metrics |
|---|---|---|---|---|
| Dual-hop hybrid FSO/RF based communication systems (both with or without HAP assisted) | Bhatnagar and Arti (2013) AF based hybrid RF/FSO satellite-terrestrial communication | GG<br>SR | Atmospheric turbulence | ASER, asymptotic ASER |
| | Zedini et al. (2016) AF based hybrid FSO/RF communication | GG<br>Nakagami-m | Atmospheric turbulence, pointing error, FSO receiver type | OP, ergodic capacity, BER - BPSK |
| | Chen et al. (2019) AF based hybrid FSO/RF communication with energy harvesting | GG<br>Rayleigh | Atmospheric turbulence, pointing error | OP |
| | Ahmad et al. (2017) Hybrid FSO/RF basedsatellite communication with optical feeder link | LN<br>Double-LN | Atmospheric turbulence, pointing error, multiantenna | OP, ergodic capacity, ABER - PSK, SQAM |
| | Zedini et al. (2020) Hybrid FSO/RF based satellite communication | GG<br>SR | Atmospheric turbulence, pointing error, multiantenna, FSO receiver type, HPA nonlinearity | OP, ergodic capacity, ABER - PSK, SQAM |
| | Sharma et al. (2019) Switching-based hybrid FSO/RF system with MRC receiver | GG<br>Nakagami-m | Atmospheric turbulence, path-loss | OP, ASER-SQAM |
| | Li et al. (2019) NOMA based multiuser hybrid FSO/RF communication | $\mathcal{M}$<br>Nakagami-m | Atmospheric turbulence, pointing error, multiuser | OP, asymptotic OP, data-rate (capacity) |
| | Kong et al. (2020) Multiuser UAV assisted DF based HSTN | GG<br>Rayleigh | Atmospheric turbulence, path-loss, multiantenna, multiuser | Ergodic capacity |
| | Swaminathan et al. (2021) HAP assisted switching based uplink RF/FSO ground to satellite communication | GG<br>SR | Atmospheric turbulence, path-loss, pointing error, FSO receiver type | OP, asymptotic OP, ASER - MPSK |
| | Singya and Alouini (2021) HAP assisted downlink hybrid FSO/RF based satellite-terrestrial communication | GG<br>Nakagami-m | Atmospheric turbulence, pointing error, FSO receiver type, multiantenna, multiuser, outdated CSI | OP, asymptotic OP, ergodic capacity, effective capacity, ASER- HQAM, XQAM, RQAM, SQAM |
| | Xu and Song (2021) UAV assisted RF/FSO communication | $\kappa - \mu$<br>$\mathcal{M}$ | Atmospheric turbulence, pointing error, FSO receiver type | OP, asymptotic OP, ergodic capacity, ABER - BPSK, DPSK, asymptotic ABER |
| | Xu and Song (2020) Hybrid RF/FSO based communication | $\kappa - \mu$<br>$\mathcal{M}$ | Atmospheric turbulence, pointing error, FSO receiver type | OP, asymptotic OP, ergodic capacity, ABER - BPSK, DPSK, asymptotic ABER |
| | Xu and Zhang (2021) AF based RF/FSO deep space communication | EW<br>Nakagami-m | Solar scintillation effect | OP, ergodic capacity, ABER - MPSK |
| Multi-hop mixed FSO/RF based Communication Systems | Altubaishi and Alhamawi (2019) AF based multi-hop hybrid FSO/RF communication | GG<br>Rayleigh | Atmospheric turbulence, pointing error, path-loss | Ergodic capacity, |
| | Ashrafzadeh et al. (2020) AF based multi-hop FSO communication | GG | Atmospheric turbulence, pointing error, FSO receiver type | OP, asymptotic OP, ABER |
| | Zedini and Alouini (2015) AF based multi-hop FSO communication | GG | Atmospheric turbulence, pointing error | OP, ergodic capacity, asymptotic ergodic capacity, ABER-OOK |
| | Datsikas et al. (2010) AF based serial multi-hop FSO communication | GG | Atmospheric turbulence, | OP, ABER - BPSK, DPSK, asymptotic ABER |
| | Wang et al. (2015) DF based multi-hop FSO communication system | EW | Atmospheric turbulence | OP, ABER - BPSK |
| Multi-hop LAP/HAP assisted mixed FSO/RF based communication Systems | Yang et al. (2018) LAP based multi-hop RF/FSO/RF communication | GG<br>Rician | Atmospheric turbulence pointing error | OP |
| | Sharma et al. (2016) HAP assisted multi-hop FSO communication | GG | Atmospheric turbulence, pointing error, path-loss | ABER, average channel, capacity |
| | Michailidis et al. (2018) Mixed RF/FSO/RF based triple-hop communication | GG<br>Rician | Atmospheric turbulence pointing error | OP |
| Our Work | Multiple serial HAPs assisted mixed FSO/RF based multiuser multiantenna communication system | GG<br>Nakagami-m | Atmospheric turbulence, pointing error, FSO receiver type, multiantenna, multiuser | OP, asymptotic OP, ABER - OOK, MPSK, MQAM |

GG - Gamma-Gamma
LN - Log-normal
EW - Exponentiated Weibull
$\mathcal{M}$ - Malaga distribution
HQAM - Hexagonal QAM
XQAM - Cross QAM
RQAM - Rectangular QAM
OP - Outage probability
ABER - Average bit-error-rate
MPSK - M-ary phase shift keying
MQAM- M-ary quadrature amplitude modulation

hop FSO/RF system. In (Wang et al., 2015), authors have discussed the performance of multi-hop exponentiated Weibull distributed FSO system. However, above discussed multi-hop works focus only on generalized FSO systems without including HAP networks.

On the other hand, HAPs are having a wide 500 km radius footprint as recommended by International Telecommunication Union (ITU) (ITU-Radiocommun, 2000). Further, most of the HAP assisted projects have smaller coverage area and combining multiple HAPs can provide coverage to even entire country. For example, authors in (Miura and Oodo, 2001) and (Milas et al., 2003) have proposed respectively 16 and 18 HAPs configurations to provide coverage to entire Japan and Greece. However, only few works focus on the performance of multi-hop HAP/LAP assisted communication system. In (Yang et al., 2018), outage probability of LAP assisted RF/FSO/RF multi-hop system is derived. In (Sharma et al., 2016), authors have evaluated the performance of inter-HAP FSO communication system. Authors in (Michailidis et al., 2018) have discussed the performance of a three-hop HAP assisted RF/FSO/RF communication system. The above discussed works are summarized in **Table 1** in details. The various considerations, channel models, and derived performance metrics are shown in **Table 1** which are compared with our work (highlighted in bold letters) to show the novelty of our work.

As discussed above, we have seen significant works on dual-hop hybrid FSO/RF based systems. However, very limited work is seen on HAP assisted multi-hop hybrid FSO/RF scenario. Motivated with this, in this work, a highly reliable, robust, and high capacity long distance multiple serial HAPs assisted mixed FSO/RF multiuser multiantenna communication system is proposed. In the proposed system, end-to-end (e2e) long distance communication is completed through high bandwidth, high capacity FSO links established between the earth station (ES) to HAP and between multiple serial HAPs situated several hundred kilometer apart, and finally to the terrestrial MUs through the RF links via multiantenna array deployed at the final HAP. The intermediate HAPs are performing selective decode-and-forward (DF) relaying. Atmospheric turbulence of the ES to HAP link is modeled with Gamma-Gamma fading along with the pointing error impairments. As HAP situates at 20 km altitude, negligible atmospheric turbulence exists hence, only pointing error is considered for the inter HAP links. A multiantenna array is deployed at the HAP and Nakagami-m fading is considered for the RF links. Further, opportunistic user scheduling is performed for the best user selection. From this prospective, the major contributions of this work are as follows:

- For the performance analysis, individual link's outage probability and overall outage probability are derived and the impact of pointing error, FSO detection type, MU selection, number of antennas, and RF fading severity are observed on the outage performance.
- To obtain the diversity order of the communication system, asymptotic outage probability is derived by performing the high SNR approximation.
- Considering various modulation schemes, a generalized average BER (ABER) expression is also derived and the impact of pointing error, FSO detection type, MU selection, number of antennas, and RF fading severity are observed on its performance.

Note that the proposed system model and the analysis shown in this work is generalized. By considering number of HAPs $N = 1$, the multi-hop serial HAPs assisted mixed FSO/RF system can be converted into a dual-hop HAP assisted mixed FSO/RF system. By considering number of users $U = 1$, the performance of *Uth* terrestrial MU can be obtained. Further, all the parameters can be adjusted and the considered system model can be deployed for various specific applications.

Rest of the work is organized as follows: In Section II, proposed system model and channel model are discussed in detail. Various performance measures like outage probability, asymptotic outage probability, and generalized ABER are discussed in detail in Section III, Section IV, and Section V, respectively. Section VI discusses various theoretical and simulation results of the proposed system and conclusions from the obtained results are finally illustrated in Section VII.

## 2 SYSTEM AND CHANNEL MODELS

### 2.1 System Model

In this work, a mixed FSO/RF based multiuser multiantenna inter-HAP configuration is considered to provide high data-rates to the terrestrial MUs as shown in **Figure 1**. We have considered a communication scenario, where a source ES is communicating to the terrestrial MUs which are far apart through the use of multiple serial HAPs. Initially, the ES transmits the optical signal $s(t)$ to HAP in first time slot. Hence, the received optical signal at the first HAP can be expressed as

$$y_H(t) = \left(P_s \eta \delta_{EH} I\right)^{r/2} s(t) + n_{EH}(t), \tag{1}$$

where $\eta$ is the optical-to-electrical conversion coefficient and $r$ decides the type of FSO detector, wherein $r = 1$ corresponds to the heterodyne detection and $r = 2$ represents the IM/DD. Here $I = I_a I_p$ represents the fading coefficient of the FSO link, where $I_a$ is the fading due to atmospheric turbulence and $I_p$ represents the pointing error associated with the FSO link. Further, $n_{EH}(t) \sim \mathcal{N}(0, \sigma_o^2)$ represents the additive white Gaussian noise (AWGN) with zero mean and $\sigma_o^2$ variance associated with the ES to HAP link. The noise variance is $\sigma_0^2 = KB_oT_o$, where $K = 1.38 \times 10^{-23}$ is the Boltzmann constant, $T_o$ represents the noise temperature in kelvin, and $B_o$ is the optical receiver bandwidth. Further, $\delta_{EH}$ represents the path-loss while transmitting the source signal from ES to HAP through the FSO link. $\delta_{EH} = \frac{G_{tE}G_{rH}}{FSL}$, where $G_{tE}$ is the ES transmitter telescope gain, $G_{rH}$ is the receiver telescope gain at the HAP, and $FSL = \frac{4\pi L}{\lambda_o}$ is the free-space loss, wherein $L$ is the ES-HAP path length and $\lambda_o$ is the optical signal wavelength. A 1550 nm

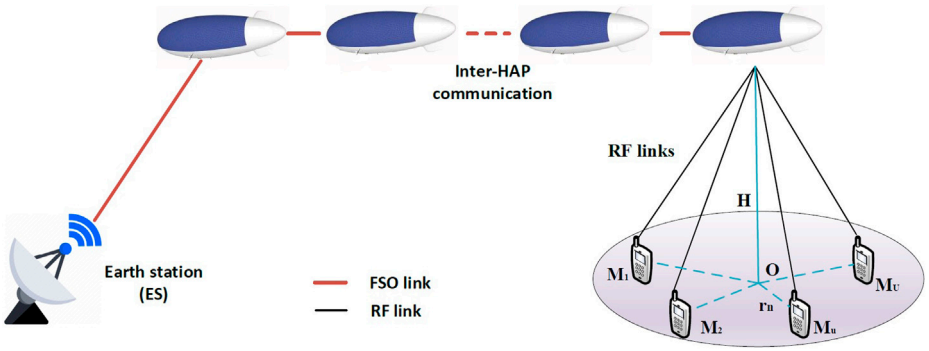


**FIGURE 1 |** Considered system model.

wavelength optical beam is considered which is eye safe and most suitable due to minimum Doppler shift than other frequencies. Therefore, the instantaneous received SNR at HAP will be

$$\gamma_H = \frac{(P_s \eta \delta_{EH} I)^r}{\sigma_o^2}. \tag{2}$$

N intermediate HAPs with DF relaying are considered for e2e signal transmission. Hence, at the HAP, the received signal is first decoded, re-encoded, and then transmitted to the next HAP. The received signal can only be decoded successfully if the instantaneous received SNR at $n$th HAP is greater than or equal to the threshold SNR i.e. $\gamma_{H_n} \geq \gamma_{th}$. Hence, probability of successful detection $(\chi(\gamma_{H_n}))$ is defined as

$$\chi(\gamma_{H_n}) = \begin{cases} 0, & \text{for } \gamma_{H_n} < \gamma_{th} \\ 1, & \text{for } \gamma_{H_n} \geq \gamma_{th} \end{cases} \tag{3}$$

Let, $\hat{s}(t)$ is the decoded signal, then the optical signal received at the $n$th HAP is represented as

$$y_{H_n}(t) = \chi(\gamma_{H_{n-1}}) \left(P_{H_{n-1}} \eta \delta_{HH} I_p\right)^{r/2} \hat{s}(t) + n_{HH}(t), \tag{4}$$

where $P_{H_{n-1}}$ is the transmitted power from the $(n-1)^{th}$ HAP, $I_p$ is the FSO channel fading coefficient which only consists of pointing error and no atmospheric turbulence is considered. Further, $n_{HH}(t)$ represents the AWGN associated with the HAP-HAP link with zero mean and $\sigma_o^2$ variance. Also, $\delta_{HH} = \frac{G_{tH} G_{rH}}{FSL_{HH}}$ is the path-loss of the HAP-HAP link and considered to be same between all the HAPs. Here, $G_{tH}$ represents the gain of the transmitting telescope of the $(n-1)^{th}$ HAP and $G_{rH}$ is the receiver telescope gain of the $n$th HAP. Further, $FSL_{HH} = \frac{4\pi D}{\lambda_o}$ is the free-space loss in the HAP-HAP link, where $D$ is the inter-HAP distance. Hence, instantaneous received SNR at the $n$th HAP is given as $\gamma_{H_n} = \chi(\gamma_{H_{n-1}}) (P_{H_{n-1}} \eta \delta_{HH} I_p)^r / \sigma_o^2$.

Finally, the decoded signal from the *Nth* HAP is transmitted to the terrestrial MUs. To improve the channel capacity of the RF link and to improve its reliability, $N_t$ transmit antennas are deployed at the HAP. However, due to size limit constraint, only single antenna is assumed at the terrestrial MUs. Hence, in the last-hop, the signal received from the *Nth* HAP at the $u$th MU after transmit beamforming is given as

$$y_{M_u}(t) = \chi(\gamma_N) \sqrt{P_N} \delta_{HM_u} \mathbf{h}_u^H \mathbf{w}_u \hat{s}(t) + n_{HM_u}(t), \tag{5}$$

where $P_N$ is the *Nth* HAP's transmit power and $\chi(\gamma_N) = \prod_{n=1}^{N} \chi(\gamma_{H_n})$ is the probability of successful detection till the *Nth* HAP. Here $\mathbf{h}_u^H$ and $\mathbf{w}_u \in \mathbb{C}^{N_t \times 1}$ denote the channel vector of $N_t \times 1$ order and transmit beamforming weight vector between the *Nth* HAP and the $u$th UE, respectively. Further, $(\cdot)^H$ is a Hermitian operator and maximal ratio transmission (MRT) principle is used for the beamforming weight vector as $\mathbf{w}_u = \frac{\mathbf{h}_u}{\|\mathbf{h}_u\|_F}$, wherein $(\cdot)\|_F$ being the Frobenius norm. Further, $n_{HM_u}(t)$ represents the AWGN associated with the RF link of zero mean and $\sigma_r^2 = KT_r B_r N_F$ variance, where $K = 1.38 \times 10^{-23}$ is the Boltzmann constant, $T_r$ represents the noise temperature in kelvin, $B_r$ is the RF receiver bandwidth, and $N_F$ is the noise figure. Furthermore, $\delta_{HM_u}$ is the path-loss associated with the RF link which can be given as (Swaminathan et al., 2021)

$$\delta_{HM_u}[dB] = G_{tH} + G_{ru} - L_F - L_A - L_R - L_O, \tag{6}$$

where $G_{tH}$ is the *Nth* HAP's transmitter gain, $G_{ru}$ is the $u$th user's receiver gain, $L_F = 20\log_{10} f_{RF} + 20\log_{10} L_u + 92.45$ is the free-space loss of the RF link between the HAP and $u$th terrestrial user of $L_u$ distance (in km) with $f_{RF}$ transmission frequency, $L_A$ is the gaseous atmospheric loss, $L_R$ is the loss by rain attenuation in dB/km, and $L_O$ represents the miscellaneous losses including antenna degradation, polarization mismatch, antenna mispointing, etc. Hence, e2e instantaneous received SNR at the $u$th MU is calculated as

$$\gamma_{M_u} = \chi(\gamma_N) \frac{P_N \delta_{HU}^2 |\mathbf{w}_u^H \mathbf{h}_u|^2}{\sigma_r^2} = \chi(\gamma_N) \gamma_{HM_u}. \tag{7}$$

## 2.2 Channel Model

### 2.2.1 Earth Station to HAP Link

ES-HAP link is considered as an FSO link and its fading coefficient is characterized as $I = I_p I_a$, where $I_p$ is the pointing error and $I_a$ is the atmospheric turbulence induced fading. Let us assume, a Gaussian beam of beamwidth $\omega_L$ is propagating $L$ distance from the transmitter to receiver with $a$ aperture radius,

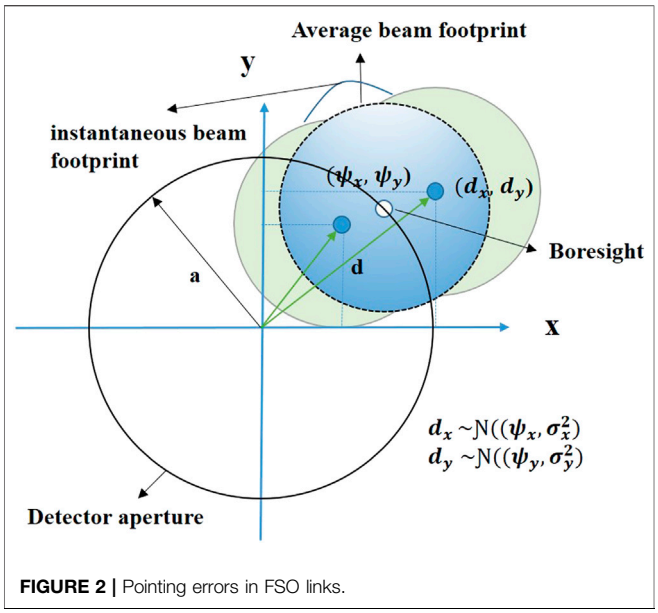


**FIGURE 2 |** Pointing errors in FSO links.

the fraction of the transmitted power collected by the receiver is approximately given as (Farid and Hranilovic, 2007)

$$I_p(r_d; L) \approx A_0 \exp\left(-\frac{2r_d^2}{\omega_{L_{eq}}^2}\right), \tag{8}$$

where $A_0$ represents the fraction of the collected power at $r_d = 0$, $r_d$ is the radial displacement between the detector and beam center, and $\omega_{L_{eq}}^2$ is the equivalent beamwidth which is given as $\omega_{L_{eq}}^2 = \frac{\sqrt{A_0\pi}}{2v_0 \exp(-v_0^2)}\omega_L^2$. Further, $A_0 = \left[\text{erf}(v_0)\right]^2$, where $v_0 = \sqrt{\frac{a^2\pi}{2\omega_L^2}}$, wherein erf(·) represents the error function. It is to be noted that the approximation (8) exists only for $\omega_L > 6a$. **Figure 2** shows various pointing errors for an FSO system. Let us consider $d_x$ and $d_y$ are the horizontal and vertical displacements of the beam in the detector plane, then $r_d = [d_x, d_y]^T$ denotes the vector for radial displacement as shown in **Figure 2**. It is assumed that $d_x$ and $d_y$ are independent and Gaussian distributed as $d_x \approx \mathcal{N}(\psi_x, \sigma_x^2)$ and $d_y \approx \mathcal{N}(\psi_y, \sigma_y^2)$, respectively. Then the amplitude of the radial vector $|d| = \sqrt{d_x^2 + d_y^2}$ is Beckmann distributed (Beckmann and Spizzichino, 1987). Thus, the pointing error of the FSO link can be modeled in various ways according to the jitter and boresight values (Jung et al., 2020).

Considering the case of identical jitters and zero boresight error, mean values $\psi_x$ and $\psi_y$ of the radial vectors $d_x$ and $d_y$ are zero and variances are identical as $\sigma_x^2 = \sigma_y^2 = \sigma^2$. Hence, the radial displacement follows Rayleigh distribution. For such case, the pointing error can be modeled as

$$f_{I_p}(x) = \frac{\epsilon^2}{A_0^{\epsilon^2}} x^{\epsilon^2 - 1}, \quad \text{for } 0 \le x \le A_0 \tag{9}$$

where $\epsilon = \frac{\omega_{L_{eq}}}{2\sigma}$ is the ratio of the equivalent beam radius to the standard deviation of jitter at the receiver.

The atmospheric turbulence $I_a$ can be modeled with Gamma-Gamma distribution, its probability density function (PDF) is given as

$$f_{I_a}(x) = \frac{2(\alpha\beta)^{(\alpha+\beta)/2}}{\Gamma(\alpha)\Gamma(\beta)} x^{(\alpha+\beta)/2-1} \text{K}_{\alpha-\beta}\left(2\sqrt{\alpha\beta x}\right), \tag{10}$$

where $\text{K}_v(\cdot)$ represents the $v$th order modified Bessel function of second kind. Further, $\alpha$ and $\beta$ are the fading coefficients of the atmospheric turbulence which are given as

$$\begin{aligned} \alpha &= \left[\exp\left(\frac{0.49\sigma_{RV}^2}{\left(1 + 1.11\sigma_{RV}^{12/5}\right)^{7/6}}\right) - 1\right]^{-1} \\ \beta &= \left[\exp\left(\frac{0.51\sigma_{RV}^2}{\left(1 + 0.69\sigma_{RV}^{12/5}\right)^{5/6}}\right) - 1\right]^{-1} \end{aligned} \tag{11}$$

where $\sigma_{RV}^2$ is the Rytov variance corresponds to the turbulence strength metric. A slant path exists between the ES and the HAP, hence, the Rytov variance for this path can be given as

$$\sigma_{RV}^2(h) = 2.25 \sec^{\frac{11}{6}}(\theta)\, k_0^{\frac{7}{6}} \int_{h_0}^{H} C_n^2(h)(h - h_0)^{\frac{5}{6}} dh, \tag{12}$$

where $\theta$ is the zenith angle, $k_0 = 2\pi/\lambda_o$ denotes the wave number, $H$ is the HAP altitude, and $h_0$ is the ES height. Further, $C_n^2$ is the refractive index structure parameter, depends upon the strength of the atmospheric turbulence and is modeled by Hufnagel-Valley model as a function of altitude $h$ which is given as

$$\begin{aligned} C_n^2(h) = {} & 0.005\,94\left(\frac{w_0}{27}\right)^2 (10^{-5}h)^{10} \exp\left(\frac{-h}{1000}\right) \\ & + 2.7 \times 10^{-16} \exp\left(\frac{-h}{1500}\right) + C_n^2(0) \exp\left(\frac{-h}{100}\right), \end{aligned} \tag{13}$$

where $C_n^2(0)$ shows the turbulence strength at ground in $\text{m}^{-2/3}$ and $w_0$ is the rms wind speed in m/s. The PDF of the FSO channel fading coefficient ($I$) can be given as

$$f_I(I) = \int f_{I|I_a}(I|I_a)\, f_{I_a}(I_a) dI_a. \tag{14}$$

Considering the identical jitters and zero boresight error case, the resulting conditional distribution is expressed as

$$f_{I|I_a}(I|I_a) = \frac{1}{I_a} f_{I_p}\left(\frac{I}{I_a}\right) = \frac{\epsilon^2}{A_0^{\epsilon^2} I_a}\left(\frac{I}{I_a}\right)^{\epsilon^2 - 1} \text{ for } 0 \le I \le A_0 I_a \tag{15}$$

Substituting (**10**) and (**15**) in (**14**), we get

$$f_I(I) = \frac{\epsilon^2}{(A_0)^{\epsilon^2}} \frac{2(\alpha\beta)^{(\alpha+\beta)/2}}{\Gamma(\alpha)\Gamma(\beta)} I^{\epsilon^2 - 1} \int_{I/A_0}^{\infty} I_a^{\frac{\alpha+\beta}{2} - \epsilon^2 - 1} \text{K}_{\alpha-\beta}\left(2\sqrt{\alpha\beta I_a}\right) dI_a. \tag{16}$$

Representing the modified Bessel function of the second kind into Meijer-G form as $\text{K}_v(x) = \text{G}_{0,2}^{2,0}\left[\frac{x^2}{4}\Big|_{v/2, -v/2}^{-,-}\right]$, solving (**16**) with the help of (Wolframe, 1998, (07.34.21.0085.01)), and after some mathematical simplifications, we get

$$f_I(I) = \frac{\epsilon^2 \alpha\beta}{A_0 \Gamma(\alpha)\Gamma(\beta)} \mathrm{G}_{1,3}^{3,0}\left[\frac{\alpha\beta}{A_0} I \middle|_{\epsilon^2-1,\alpha-1,\beta-1}^{\epsilon^2}\right]. \quad (17)$$

Instantaneous received SNR of the ES-HAP FSO link is calculated as $\gamma_H = \mu_r (I)^r$, where $r$ represents the type of FSO detector and $\mu_r$ is the average power of the FSO link. For heterodyne detection, $r = 1$, and hence, $\mu_1 = \bar{\gamma}_H$. For the IM/DD detection, $r = 2$, and hence, $\mu_2 = \frac{\epsilon^2 \alpha\beta(\epsilon^2+2)}{(\alpha+1)(\beta+1)(\epsilon^2+1)^2}\bar{\gamma}_H$. After change of variable in **(17)**, the PDF of the e2e SNR of the FSO link is given as

$$f_{\gamma_H}(x) = \frac{\epsilon^2}{r\Gamma(\alpha)\Gamma(\beta)x} \mathrm{G}_{1,3}^{3,0}\left[\frac{\alpha\beta}{A_0}\left(\frac{x}{\mu_r}\right)^{1/r} \middle|_{\epsilon^2,\alpha,\beta}^{\epsilon^2+1}\right]. \quad (18)$$

Substituting (18) in $F_{\gamma_H}(x) = \int_0^x f_{\gamma_H}(\gamma) d\gamma$ and applying (Wolframe, 1998, (07.34.21.0084.01)) with some mathematical computations, the cumulative distribution function (CDF) of the SNR of the FSO link for both the detection techniques is given as

$$F_{\gamma_H}(x) = A \mathrm{G}_{r+1,3r+1}^{3r,1}\left[\frac{B}{(A_0)^r \mu_r} x \middle|_{\varrho_2,0}^{1,\varrho_1}\right], \quad (19)$$

where $\varrho_1 = \left[\frac{\epsilon^2+1}{r}, \ldots, \frac{\epsilon^2+r}{r}\right]$, $\varrho_2 = \left[\frac{\epsilon^2}{r}, \ldots, \frac{\epsilon^2+r-1}{r}, \frac{\alpha}{r}, \ldots, \frac{\alpha+r-1}{r}, \frac{\beta}{r}, \ldots, \frac{\beta+r-1}{r}\right]$, $A = \frac{r^{(\alpha+\beta-2)}\epsilon^2}{(2\pi)^{r-1}\Gamma(\alpha)\Gamma(\beta)}$, and $B = \frac{(\alpha\beta)^r}{r^{2r}}$.

### 2.2.2 Inter HAP Links

The HAP is situated in the stratosphere above the clouds and there is almost negligible atmospheric turbulence. Hence, only the pointing error is considered between inter-HAP links. As identical jitters with zero boresight error is considered, the pointing error can be modeled by Rayleigh distribution and its PDF is given in **(9)**. Now instantaneous received SNR at the $n$th HAP for the FSO link is calculated as $\gamma_{H_n} = \bar{\gamma}_{H_n} (I_p)^r$, where $\bar{\gamma}_{H_n}$ is the average received power at the FSO detector of $n$th HAP. After change of variable in **(17)**, the PDF of the instantaneous received SNR of the HAP-HAP link is given as[1]

$$f_{\gamma_{HH}}(x) = \frac{\epsilon_o^2}{r A_0^{\epsilon_o^2}} \left(\frac{1}{\bar{\gamma}_{H_n}}\right)^{\frac{\epsilon_o^2}{r}} x^{\frac{\epsilon_o^2}{r}-1}, \text{for } 0 \le x \le \left(A_0 \bar{\gamma}_{H_n}\right)^r \quad (20)$$

Performing $F_{\gamma_{HH}}(x) = \int_0^x f_{\gamma_{HH}}(\gamma) d\gamma$, the CDF of the HAP-HAP link can be given as

$$F_{\gamma_{HH}}(x) = \begin{cases} \frac{1}{A_0^{\epsilon_o^2}} \left(\frac{x}{\bar{\gamma}_{H_n}}\right)^{\frac{\epsilon_o^2}{r}}, & \text{for } 0 \le x \le \left(A_0 \bar{\gamma}\right)^r \\ 1, & \text{else} \end{cases} \quad (21)$$

### 2.2.3 HAP to MUs RF Links

To connect the terrestrial MUs, communication between the HAP and the MUs is established through the RF links. Considering the size constraint of the MUs, single antenna is assumed at the MUs. Further, multiple transmit antennas ($N_t$) are considered at the HAP to avail the antenna diversity. The Nakagami-m distribution is considered for the RF link i.e. Nak($m$, $\Omega$), where $m$ is the fading severity and $\Omega$ is the average power of the RF link. Hence, the CDF and PDF of the $u$th MU's SNR can be given as

$$\begin{aligned} f_{\gamma_{HM_u}}(x) &= \frac{1}{\Gamma(mN_t)} \left(\frac{m}{\bar{\gamma}_U}\right)^{mN_t} x^{mN_t-1} \exp\left(-\frac{m}{\bar{\gamma}_U} x\right) \\ F_{\gamma_{HM_u}}(x) &= 1 - \frac{1}{\Gamma(mN_t)} \Gamma\left(mN_t, \frac{m}{\bar{\gamma}_U} x\right), \end{aligned} \quad (22)$$

respectively, where $\Gamma(\cdot)$ represents the complete gamma function and $\bar{\gamma}_U = \Omega \bar{\gamma}_{HM_u}$. It is considered that the terrestrial MUs are independent and identically distributed (i.i.d.) as they are close to each others. Hence, opportunistic user scheduling is performed to achive the multiuser diversity. Therefore, the instantaneous received SNR of the HAP-MU link after opportunistic scheduling is $\gamma_{HM} = \underset{u=1,2,\ldots,U}{\mathrm{Max}} \gamma_{HM_u}$. Thus, the PDF of $\gamma_{HM}$ after the order statistics is given as

$$f_{\gamma_{HM}}(x) = U\left(F_{\gamma_{HM_u}}(x)\right)^{U-1} f_{\gamma_{HM_u}}(x). \quad (23)$$

Invoking the PDF and CDF values from **(22)** in **(23)** and using the series representation of the incomplete Gamma function with multinomial expansion using (Gradshteyn and Ryzhik, 2000, (0.314)), the PDF of $\gamma_{HM}$ can be derived as

$$\begin{aligned} f_{\gamma_{HM}}(x) &= U \sum_{j=0}^{U-1} \binom{U-1}{j} (-1)^j \sum_{l=0}^{j(mN_t-1)} \\ &\times \varpi_l^j \left(\frac{m}{\bar{\gamma}_U}\right)^{mN_t+l} \frac{1}{\Gamma(mN_t)} x^{mN_t+l-1} \exp\left(-\frac{m}{\bar{\gamma}_U}(j+1)x\right), \end{aligned} \quad (24)$$

where $\varpi_l^j$ is recursively calculated as $\varpi_0^j = (\delta_0)^j$, $\varpi_1^j = j(\delta_1)$, $\varpi_l^j = \frac{1}{l\delta_0}\sum_{k=1}^{l}\left[(kj-l+k)\delta_k \varpi_{l-k}^j\right]$ for $2 \le l \le (mN_t - 1)$, $\varpi_l^j = \frac{1}{l\delta_0}\sum_{k=1}^{mN_t-1}\left[(kj-l+k)\delta_k \varpi_{l-k}^j\right]$ for $mN_t \le l < j(mN_t - 1)$, and $\varpi_{j(mN_t-1)}^j = (\delta_{mN_t-1})^j$, wherein $\delta_l = \frac{1}{l!}$ (Singya et al., 2018, 2019). Using $F_{\gamma_{HM}}(x) = \int_0^x f_{\gamma_{HM}}(\gamma) d\gamma$, the CDF of **(24)** can be obtained as

$$F_{\gamma_{HM}}(x) = U \sum_{j,l} \mathbb{C}_0 \mathbb{C}_2^{-\mathbb{C}_1} \Upsilon(\mathbb{C}_1, \mathbb{C}_2 x), \quad (25)$$

where $\sum_{j,l} = \sum_{j=0}^{U-1} \sum_{l=0}^{j(mN_t-1)}$, $\mathbb{C}_0 = U\binom{U-1}{j}(-1)^j \varpi_l^j \left(\frac{m}{\bar{\gamma}_U}\right)^{mN_t+l} \frac{1}{\Gamma(mN_t)}$, $\mathbb{C}_1 = mN_t + l$, and $\mathbb{C}_2 = \frac{m}{\bar{\gamma}_U}(j+1)$.

## 3 OUTAGE PROBABILITY

Outage probability is one of the important performance measures and defines the probability of reaching the instantaneous e2e SNR below a fixed threshold ($\gamma_{th}$). For the considered system, e2e instantaneous received SNR is shown in **(7)**, hence the overall outage probability is given as

$$\begin{aligned} \mathcal{P}_o(\gamma_{th}) = 1 - &\underbrace{\left(1 - F_{\gamma_H}(\gamma_{th})\right)}_{\text{ES–HAP}} \underbrace{\left(1 - F_{\gamma_{HH}}(\gamma_{th})\right)^{N-1}}_{\text{HAP–HAP}} \\ &\times \underbrace{\left(1 - F_{\gamma_{HM}}(\gamma_{th})\right)}_{\text{HAP–EU}}. \end{aligned} \quad (26)$$

[1]Please note that $\epsilon_o$ is same as $\epsilon$, related to the severity of pointing error. However, $\epsilon_o$ shows the severity of pointing error of the inter-HAP links which is different than $\epsilon$ related to the ES-HAP link's pointing error severity because different selection parameters are considered for both the links.

Substituting the respective CDF values of the individual links in **(26)**, we get

$$\mathcal{P}_o(\gamma_{th}) = 1 - \left(1 - AG_{r+1,3r+1}^{3r,1}\left[\frac{B}{(A_0)^r\mu_r}\gamma_{th}\middle|_{\varrho_2,0}^{1,\varrho_1}\right]\right) \times \left(1 - \frac{1}{A_0^{\epsilon_o^2}}\left(\frac{\gamma_{th}}{\bar{\gamma}_{H_n}}\right)^{\frac{\epsilon_o^2}{r}}\right)^{N-1}\left(1 - U\sum_{j,l}\mathbb{C}_0\mathbb{C}_2^{-\mathbb{C}_1}\Upsilon(\mathbb{C}_1, \mathbb{C}_2\gamma_{th})\right). \tag{27}$$

Using the binomial series expansion and after some mathematical computations, (**27**) can be solved as

$$\begin{aligned}\mathcal{P}_o(\gamma_{th}) = \Bigg[&AG_{r+1,3r+1}^{3r,1}\left[\frac{B}{(A_0)^r\mu_r}x\middle|_{\varrho_2,0}^{1,\varrho_1}\right] - \sum_{z=1}^{N-1}\binom{N-1}{z}(-1)^z\frac{1}{A_0^{\epsilon_o^2 z}}\left(\frac{\gamma_{th}}{\bar{\gamma}_{H_n}}\right)^{\frac{\epsilon_o^2 z}{r}}\\ &+U\sum_{j,l}\mathbb{C}_0\mathbb{C}_2^{-\mathbb{C}_1}\Upsilon(\mathbb{C}_1, \mathbb{C}_2\gamma_{th})\\ &+U\sum_{j,l}\sum_{z=1}^{N-1}\binom{N-1}{z}(-1)^z\frac{1}{A_0^{\epsilon_o^2 z}}\mathbb{C}_0\mathbb{C}_2^{-\mathbb{C}_1}\left(\frac{1}{\bar{\gamma}_{H_n}}\right)^{\frac{\epsilon_o^2 z}{r}}(\gamma_{th})^{\frac{\epsilon_o^2 z}{r}}\Upsilon(\mathbb{C}_1, \mathbb{C}_2\gamma_{th})\\ &+A\sum_{z=1}^{N-1}\binom{N-1}{z}(-1)^z\frac{1}{A_0^{\epsilon_o^2 z}}\left(\frac{\gamma_{th}}{\bar{\gamma}_{H_n}}\right)^{\frac{\epsilon_o^2 z}{r}}G_{r+1,3r+1}^{3r,1}\left[\frac{B}{(A_0)^r\mu_r}x\middle|_{\varrho_2,0}^{1,\varrho_1}\right]\\ &-AU\sum_{j,l}\mathbb{C}_0\mathbb{C}_2^{-\mathbb{C}_1}\Upsilon(\mathbb{C}_1, \mathbb{C}_2\gamma_{th})G_{r+1,3r+1}^{3r,1}\left[\frac{B}{(A_0)^r\mu_r}x^{1,\varrho_1}_{\varrho_2,0}\right]\\ &-AU\sum_{j,l}\sum_{z=1}^{N-1}\binom{N-1}{z}(-1)^z\frac{1}{A_0^{\epsilon_o^2 z}}\mathbb{C}_0\mathbb{C}_2^{-\mathbb{C}_1}\left(\frac{1}{\bar{\gamma}_{H_n}}\right)^{\frac{\epsilon_o^2 z}{r}}(\gamma_{th})^{\frac{\epsilon_o^2 z}{r}}\Upsilon(\mathbb{C}_1, \mathbb{C}_2\gamma_{th})\\ &\times G_{r+1,3r+1}^{3r,1}\left[\frac{B}{(A_0)^r\mu_r}x\middle|_{\varrho_2,0}^{1,\varrho_1}\right]\Bigg].\end{aligned} \tag{28}$$

## 4 ASYMPTOTIC OUTAGE PROBABILITY

Various insights on the system's performance can be highlighted through the obtained outage probability (**28**). However, (**28**) is quite complex to decide the diversity order of the considered system. Hence, in this Section, we have conducted asymptotic analysis on the outage probability to obtain the diversity order. For this, the transmit SNR is assumed to tend to infinity. Therefore, at high SNR, (**26**) can be approximated as

$$\mathcal{P}_o^A(\gamma_{th}) \approx F_{\gamma_H}^A(\gamma_{th}) + (N-1)\times F_{\gamma_{HH}}^A(\gamma_{th}) + F_{\gamma_{HM}}^A(\gamma_{th}). \tag{29}$$

Corollary 1: By using the identities as shown in **(34)** and **(35)**, asymptotic outage probability for the considered system is expressed as

$$\begin{aligned}\mathcal{P}_o^A(\gamma_{th}) \approx{}& A\sum_{p=1}^{3r}\left(\frac{B\gamma_{th}}{(A_0)^r\mu_r}\right)^{\varrho_4,p}\\ &\frac{\prod_{q=1,q\neq p}^{3r}\Gamma(\varrho_{4,q}-\varrho_{4,p})\prod_{q=1}^{1}\Gamma(1-\varrho_{3,q}+\varrho_{4,p})}{\prod_{q=2}^{r+1}\Gamma(\varrho_{3,q}-\varrho_{4,p})\prod_{3r+1}^{3r+1}\Gamma(1-\varrho_{4,q}+\varrho_{4,p})}\\ &+\frac{(N-1)}{A_0^{\epsilon_o^2}}\left(\frac{\gamma_{th}}{\bar{\gamma}_{H_n}}\right)^{\frac{\epsilon_o^2}{r}}+\left(\frac{1}{\Gamma(mN_t+1)}\right)^U\left(\frac{m\gamma_{th}}{\bar{\gamma}_U}\right)^{UmN_t}.\end{aligned} \tag{30}$$

**TABLE 2 |** Selection parameters for various modulation schemes (Zedini et al., 2020).

| Modulation | $n_0$ | $\kappa$ | $g_p$ |
|---|---|---|---|
| OOK | 1 | 1 | 1/2 |
| BPSK | 1 | 1 | 1 |
| M-PSK | $\mathrm{Max}\left(\frac{M}{4}, 1\right)$ | $\frac{2}{\mathrm{Max}(2,\log_2(M))}$ | $\sin^2\left(\frac{(2p-1)\pi}{M}\right)$ |
| M-QAM | $\sqrt{M}/2$ | $\frac{4}{\log_2(M)}\left(1-1/\sqrt{M}\right)$ | $\frac{3(2p-1)^2}{2(M-1)}$ |

From **(34)**, we observed that $\min\left(\frac{\epsilon^2}{r}, \frac{\alpha}{r}, \frac{\beta}{r}\right)$ is the dominant term of meijer-G function. Hence, the diversity order of the overall system is given as $\min\left(\frac{\epsilon^2}{r}, \frac{\alpha}{r}, \frac{\beta}{r}, \frac{\epsilon_o^2}{r}, UmN_t\right)$.
Proof: See the **Appendix**.

## 5 AVERAGE BER ANALYSIS

For various modulation schemes, a generalized ABER expression for the considered communication system can be given as (Zedini et al., 2020)

$$\mathcal{P}_e = \frac{\kappa}{2\Gamma(1/2)}\sum_{p=1}^{n_0}\sqrt{g_p}\int_0^\infty x^{-1/2}e^{-g_p x}\mathcal{P}_o(\gamma)d\gamma, \tag{31}$$

where $n_0$, $\kappa$, and $g_p$ are the selection parameters for various modulation schemes and their values are shown in **Table 2**.

Please note that by using the IM/DD, we can obtain the ABER performance of on-off keying (OOK), preferred commonly in practical FSO systems as it is flexible to laser nonlinearity with ease of use. Further, we have analyzed the ABER performance of various MPSK (including the BPSK) and MQAM schemes using the coherent heterodyne detection at FSO receivers. Now plugin (**28**) in (**31**), and performing various mathematical computations by using (Gradshteyn and Ryzhik, 2000, (3.351),(6.455),(7.813), (8.352)) to solve the integrals, the final generalized analytical ABER expression is derived as

$$\mathcal{P}_e = \frac{\kappa}{2\Gamma(1/2)}\sum_{p=1}^{n}\sqrt{g_p}\left[I_1 - I_2 + I_3 + I_4 + I_5 - I_6 - I_7\right], \tag{32}$$

where

$$\begin{aligned}I_1 &= A\mathbb{F}_1\left(\frac{1}{2}, g_p\right),\\ I_2 &= \sum_{z=1}^{N-1}\binom{N-1}{z}\frac{(-1)^z}{A_0^{\epsilon_o^2 z}}\left(\frac{1}{\bar{\gamma}_{H_n}}\right)^{\frac{\epsilon_o^2 z}{r}}\Gamma\left(\frac{\epsilon_o^2 z}{r}+\frac{1}{2}\right)g_p^{-\left(\frac{\epsilon_o^2 z}{r}+\frac{1}{2}\right)},\\ I_3 &= U\sum_{j,l}\mathbb{C}_0\mathbb{C}_2^{-\mathbb{C}_1}\mathbb{F}_2\left(\frac{1}{2}, g_p\right),\\ I_4 &= U\sum_{j,l}\mathbb{C}_0\mathbb{C}_2^{-\mathbb{C}_1}\sum_{z=1}^{N-1}\binom{N-1}{z}\frac{(-1)^z}{A_0^{\epsilon_o^2 z}}\left(\frac{1}{\bar{\gamma}_{H_n}}\right)^{\frac{\epsilon_o^2 z}{r}}\mathbb{F}_2\left(\frac{\epsilon_o^2 z}{r}+\frac{1}{2}, g_p\right),\\ I_5 &= A\sum_{z=1}^{N-1}\binom{N-1}{z}\frac{(-1)^z}{A_0^{\epsilon_o^2 z}}\left(\frac{1}{\bar{\gamma}_{H_n}}\right)^{\frac{\epsilon_o^2 z}{r}}\mathbb{F}_1\left(-\frac{\epsilon_o^2 z}{r}+\frac{1}{2}, g_p\right),\\ I_6 &= AU\sum_{j,l}\mathbb{C}_0\mathbb{C}_2^{-\mathbb{C}_1}\Gamma(\mathbb{C}_1)\left[\mathbb{F}_1\left(\frac{1}{2}, (\mathbb{C}_2+g_p)\right) - \sum_{z_1=0}^{\mathbb{C}_1-1}\frac{\mathbb{C}_2^{z_1}}{z_1!}\mathbb{F}_1\left(-z_1+\frac{1}{2}, (\mathbb{C}_2+g_p)\right)\right],\\ I_7 &= AU\sum_{j,l}\mathbb{C}_0\mathbb{C}_2^{-\mathbb{C}_1}\sum_{z=1}^{N-1}\binom{N-1}{z}\frac{(-1)^z}{A_0^{\epsilon_o^2 z}}\left(\frac{1}{\bar{\gamma}_{H_n}}\right)^{\frac{\epsilon_o^2 z}{r}}\Gamma(\mathbb{C}_1)\\ &\quad\times\left[\mathbb{F}_1\left(-\frac{\epsilon_o^2 z}{r}+\frac{1}{2}, (\mathbb{C}_2+g_p)\right) - \sum_{z_1=0}^{\mathbb{C}_1-1}\frac{\mathbb{C}_2^{z_1}}{z_1!}\mathbb{F}_1\left(-\frac{\epsilon_o^2 z}{r}-z_1+\frac{1}{2}, (\mathbb{C}_2+g_p)\right)\right],\end{aligned} \tag{33}$$

**TABLE 3 |** Various parameters of interest.

| Parameter | Value |
|---|---|
| Earth station height ($h_0$) | 1 m |
| HAP altitude ($H$) | 20 km |
| Number of HAPs ($N$) | 6 |
| Inter HAP distance ($D$) | 300 km |
| Zenith angle ($\theta$) | $\pi/6$ |
| Optical wavelength ($\lambda_o$) | 1550 nm |
| Wind speed ($w_0$) | 21 m/s |
| Turbulence strength at ground level ($C_n^2(0)$) | $5 \times 10^{-13}$ $m^{-2/3}$ |
| Parameters related to the pointing error of ES-HAP link ($a$, $\omega_L$, $\sigma$) | 10 cm, 50 cm, 10 cm |
| Parameters related to the pointing error of HAP-HAP link ($a$, $\omega_L$, $\sigma$) | 10 cm, 30 cm, 7 cm |
| Transmit and receive telescope gain for ES-HAP link ($G_{tE}$, $G_{rH}$) | 5 dB, 10 dB |
| Transmit and receive telescope gain for HAP-HAP link ($G_{tH}$, $G_{rH}$) | 10 dB, 15 dB |
| Transmit and receive telescope gain for HAP-MUs link ($G_{tH}$, $G_{rU}$) | 28 dB, 10 dB |
| Optical receiver bandwidth ($B_o$) | 30 GHz, |
| RF receiver bandwidth ($B_r$) | 20 MHz |
| Noise temperature at optical and RF receivers ($T_o$, $T_r$) | 300 K, 58 K |
| Noise figure | 2 dB |
| Various attenuation losses in RF propagation link | $L_A$= $5.4 \times 10^{-3}$ dB/km, $L_R$= 0.01 dB/km, $L_O$ = 2 dB |

wherein $\mathbb{F}_1(\phi_1,\phi_2) = (\phi_2)^{\phi_1-1} G_{r+1,3r+1}^{3r,1}\left[\frac{B}{\phi_2(A_0)^r\mu_r}x\Big|_{\varrho_2,0}^{\phi_1,1,\varrho_1}\right]$ and $\mathbb{F}_2(\phi_1,\phi_2) = \mathbb{C}_2^{\mathbb{C}_1}\frac{\Gamma(\mathbb{C}_1+\phi_1)}{\mathbb{C}_1(\mathbb{C}_2+\phi_2)^{\mathbb{C}_1+\phi_1}}\,{}_2F_1\left(1,\mathbb{C}_1+\phi_1;\mathbb{C}_1+1,\frac{\mathbb{C}_2}{\mathbb{C}_2+\phi_2}\right)$.

## 6 THEORETICAL AND SIMULATION RESULTS

In this Section, numerical values from the derived results are obtained and are validated through the simulations performed through Matlab by conducting $10^8$ realizations. The atmospheric turbulence of ES-HAP link is generated by the product of two generalized Gamma distributed random variables. The radial displacement parameter is considered to be Rayleigh distributed and is applied to (**8**) for pointing error impairments. Throughout the analysis, $\eta = 1$ is considered. Unity transmit power is considered at all the nodes and $\gamma_{th} = 1$ dB is considered for the analysis. Further, parameters related to various links are shown in **Table 3** unless otherwise stated.

In **Figure 3**, analytical and simulation results of outage probability against transmit SNR are shown for all three links. In **Figure 3A**, analytical and simulation results of ES-HAP link are compared for both the IM/DD and heterodyne detection (Het. in figures) techniques for different atmospheric turbulence conditions based on various ground turbulence i.e. $C_n^2(0) = 1.7 \times 10^{-14}$, $C_n^2(0) = 5 \times 10^{-13}$, and $C_n^2(0) = 1 \times 10^{-12}$, (in $m^{-2/3}$) respectively for weak, moderate, and strong ground turbulence conditions. Simulation results match well with the analytical results and validate the accuracy. From **Figure 3A**, we observe a significant improvement in outage performance while going from strong to weak turbulence for both the detection techniques. Also, heterodyne detection provides significant performance improvement than IM/DD due to its capability in handling turbulence effects more efficiently despite having implementation complexity (Zedini et al., 2016). For the performance analysis, $a$ = 10 cm, $\omega_L = 50$ cm, and $\sigma = 10$ cm are considered which corresponds to $\epsilon = 2.553$. The same can be conducted for different values of $\epsilon$ by varying these selection parameters to show the impact of pointing error.

In **Figure 3B**, analytical and simulation results of HAP-HAP link are compared for various values of $\omega_L/a$ which corresponds to different values of $\epsilon_o$. Simulation results match well with the analytical results and validate the accuracy. Further, selection of appropriate values of $a$, $\omega_L$, and $\sigma$ results in an appropriate $\epsilon_o$ for desired system performance. **Figure 3C** compares the analytical and simulation results of HAP to terrestrial MUs link for different values of fading severity $m$, number of antenna $N_t$, and number of terrestrial users $U$. $U = 1$ gives the performance of $u$th terrestrial MU while increasing $U$ gives the flexibility of user selection. Considering $U = 1$, $m = 1$, $N_t = 1$ as a reference case, we observe significant performance improvement while increasing $m$ or $N_t$ or both. However, increase in $N_t$ gives better performance than increase in $m$. Increase in $U$ provides the user selection flexibility and improves the outage performance further.

In **Figure 4**, analytical, simulation, and asymptotic results of overall system outage probability are compared for various values of $U$, $m$, and $N_t$ while heterodyne detection is considered at FSO receiver. For the analysis, $C_n^2(0) = 5 \times 10^{-13}$ $m^{-2/3}$ is considered and $\omega_L/a = 5$ for moderate pointing error (**Figure 4A**) and $\omega_L/a = 2$ for severe pointing error (**Figure 4B**) are considered. Rest of the parameters are shown in **Table 3**. From **Figure 4A**, considering $U = 1$, $m = 1$, $N_t = 1$ as reference case, for an outage probability of $10^{-2}$, approximately 8.7 and 11.7 dB gains are achieved while increasing $m$ from one to two and $N_t$ from 1 to 2, respectively. This indicates better performance with an increase in $N_t$ than $m$ by approximately 3 dB. Further, the gain is same throughout the SNR range except for $U = 1$, $m = 2$, $N_t = 2$ and $U = 2$, $m = 2$, $N_t = 2$ cases. For $U = 2$, $m = 2$, $N_t = 2$, there must be a significant performance improvement as shown in **Figure 3C**, however, only slight improvement is observed over $U = 1$, $m = 2$, $N_t = 2$. This is because the ES-HAP FSO link's performance reaches to its saturation which limits the overall outage performance. Hence, no further performance improvement is achieved with the increase in $U$, $m$, and $N_t$ beyond $U = 2$, $m = 2$, $N_t = 2$ case. In **Figure 4B**, $\omega_L/a = 2$ is maintained for the FSO links for severe pointing error case. From **Figure 4B**, by considering $U = 1$, $m = 1$, $N_t = 1$ as reference case, we can observe a clear performance improvement for $U = 1$, $m = 2$, $N_t = 1$ or

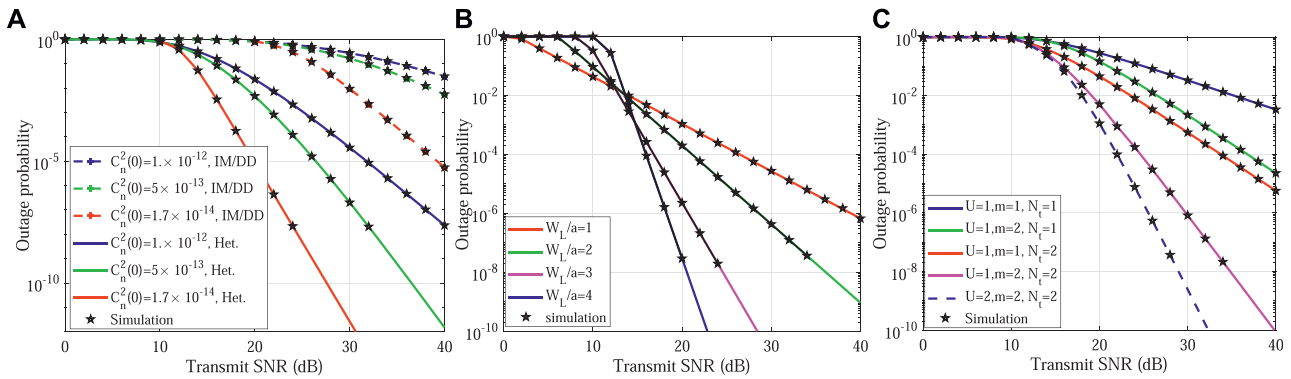


**FIGURE 3 |** Comparison of analytical and simulation results of individual link's outage probability against transmit SNR for **(A)** ES-HAP link, **(B)** HAP-HAP link, and **(C)** HAP-MUs link.

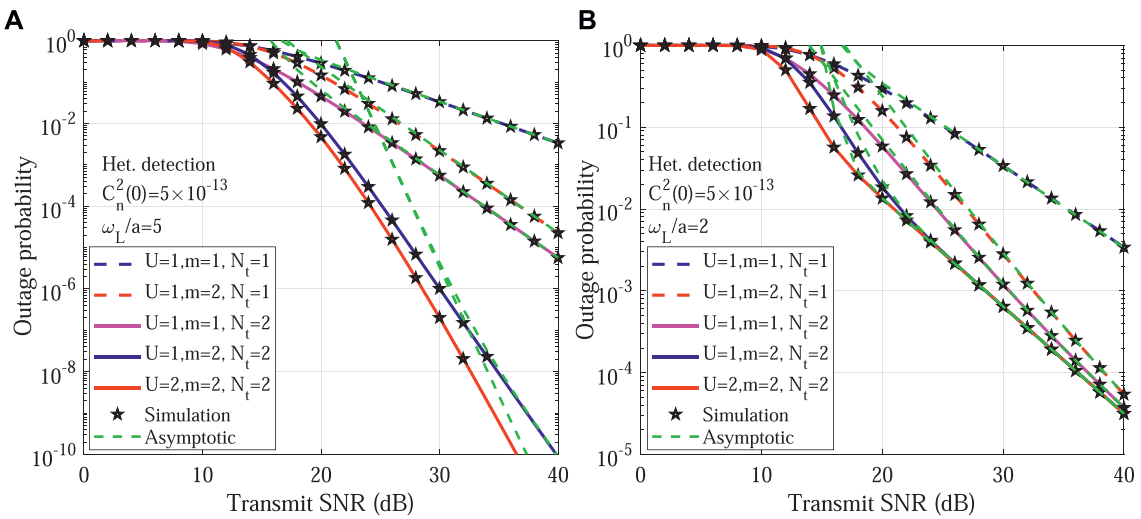


**FIGURE 4 |** Analytical, simulation, and asymptotic results of overall outage probability against transmit SNR for **(A)** Moderate pointing error and **(B)** Severe pointing error.

$U = 1$, $m = 1$, $N_t = 2$. For further increase in $U$, $m$, or $N_t$, we can observe slight improvement only in the low and medium SNR range. However, no such improvement can be seen at high SNRs and all the curves merge with each other. This is because the ES-HAP FSO link's performance saturates early due to severe pointing error which limits the overall outage performance. Simulation results validate the analytical results presented in **Figure 4**. Further, asymptotic results on outage probability are also shown in **Figure 4** which match with the outage results at high SNRs for all the considered cases and validates the high SNR approximation. Further, the diversity order of the overall system is obtained as $\min\left(\frac{\epsilon^2}{r}, \frac{\alpha}{r}, \frac{\beta}{r}, \frac{\epsilon_o^2}{r}, UmN_t\right)$.

In **Figure 5**, analytical and simulation results of ABER for 4-QAM are compared for various values of $U$, $m$, and $N_t$ while heterodyne detection is considered at the FSO receiver. For the analysis, $C_n^2(0) = 5 \times 10^{-13}$ $\mathrm{m}^{-2/3}$ is considered and $\omega_L/a = 5$ for moderate pointing error (**Figure 5A**) and $\omega_L/a = 2$ for severe pointing error (**Figure 5B**) are considered. Rest of the parameters are shown in **Table 3**. From **Figure 5A**, a significant improvement in ABER performance is observed with the increase in $m$, $N_t$, $U$ or all as compared to the $U = 1$, $m = 1$, $N_t = 1$ reference case. Further, simulation results validate the derived analytical results. Considering $U = 1$, $m = 1$, $N_t = 1$ as a reference case, for an ABER of $10^{-2}$, approximately 5.2 and 8.1 dB gains achieved while increasing $m$ from one to two and $N_t$ from 1 to 2, respectively. Hence, increase in $N_t$ gives nearly 2.9 dB gain than the increase in $m$. Also for $U = 2$, $m = 2$, $N_t = 2$, only marginal improvement is observed over the $U = 1$, $m = 2$, $N_t = 2$ case. This is due to the fact that the ES-HAP FSO link's performance reaches to its saturation which limits the overall ABER performance. Hence, no further performance improvement is achieved with the increase in $U$, $m$, and $N_t$ beyond $U = 2$, $m = 2$, $N_t = 2$ case. In **Figure 5B**, $\omega_L/a = 2$ is maintained for the FSO links for severe pointing error case. From **Figure 5B**, by considering $U = 1$, $m = 1$, $N_t = 1$ as reference case, we can observe a clear ABER performance improvement for $U = 1$, $m = 2$, $N_t = 1$ or $U = 1$, $m = 1$, $N_t = 2$. However, for further increase in $U$, $m$,

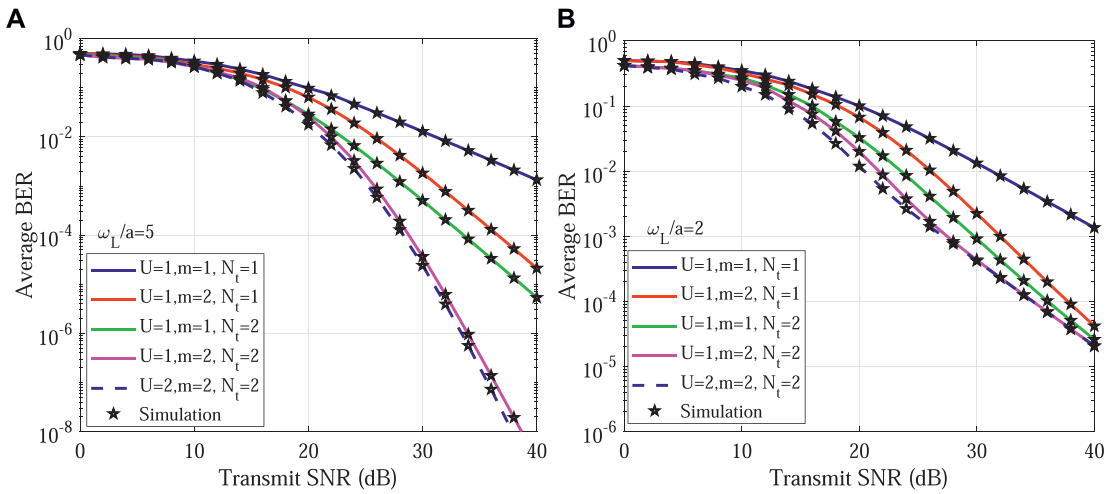


**FIGURE 5 |** Analytical and simulation results of ABER against transmit SNR for 4-QAM with heterodyne detection at FSO receiver for **(A)** Moderate pointing error and **(B)** Severe pointing error.

or $N_t$, we can observe slight improvement only in the low and medium SNR range. However, no so such improvement can be seen at high SNRs and all the curves merge with each other. This is because the ES-HAP FSO link's performance saturates early due to severe pointing error which limits the overall ABER performance. Further, simulation results validate the analytical results presented in **Figure 5** for all the cases.

In **Figure 6**, ABER of various modulation schemes are compared against transmit SNR. For OOK modulation, IM/DD detection is considered at the FSO receiver while heterodyne detection is preferred for the rest of the complex modulation schemes. For the analysis, $U = 1$, $m = 1$, and $N_t = 2$ are considered and other parameters are mentioned in **Table 3**. It is observed that BPSK provides significant gain in ABER performance than OOK as heterodyne detection provides significant performance improvement over IM/DD. To achieve an ABER of $10^{-2}$, BPSK provides around 15 dB gain over the OOK. Further, it is observed that the ABER performance of 4-QAM is same as 4-PSK. However, with the increase in constellation order, MQAM outperforms the MPSK. For an ABER of $10^{-3}$, 16-QAM provides approximately 3.2 dB gain over the 16-PSK. This gain improves further with the increase in M.

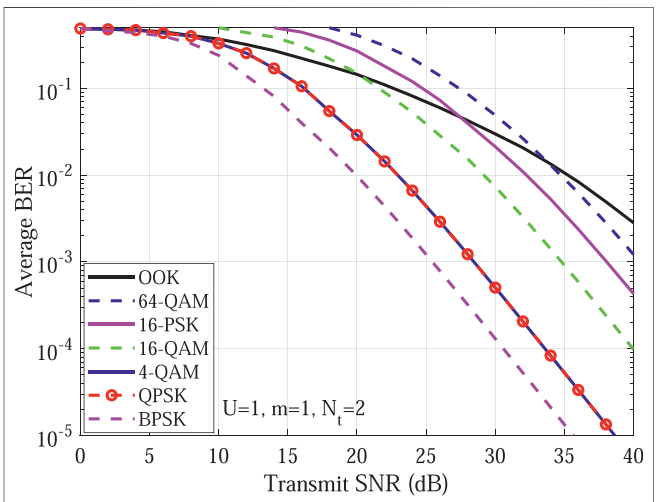


**FIGURE 6 |** ABER comparison for various modulation schemes.

## 7 CONCLUSION

In this work, a mixed FSO/RF based multiple serial HAPs assisted multiuser multiantenna terrestrial communication system was considered, where ES-HAP and HAP-HAP links were FSO links and HAP to terrestrial MUs link was an RF link. Both the heterodyne detection and IM/DD techniques were considered at FSO receivers. The atmospheric turbulence of ES-HAP link was modeled with gamma-gamma fading with pointing error impairments. The HAP-HAP links were assumed to have pointing errors only. Multiantenna array was considered at the *Nth* HAP and best user selection was performed to improve the performance of RF links for the terrestrial users which were Nakagami-m distributed. For the performance analysis, analytical expressions of individual link's outage probability, overall outage probability, asymptotic outage probability, and a generalized ABER expression of various modulation schemes were derived. Finally, the impact of various selection parameters like pointing error, FSO detection type, MU selection, RF fading severity, and the number of antennas were observed on their performance. The proposed system model and the analysis shown in this work is generalized. All the parameters can be adjusted and the considered system model can be deployed for various specific wireless communication applications. By considering number of HAPs equal to one, the multi-hop serial HAPs assisted hybrid FSO/RF system can be converted

into a dual-hop HAP assisted hybrid FSO/RF system which can be applied for a short range highly reliable and robust high data-rate communication for various wireless applications including the emergency disastrous situations, temporary mass events, and even in military applications. By considering $N$ HAPs in a serial mode, the coverage for the communication can be improved till several hundred kilometers and the problem of connecting the unconnected can be solved.

## DATA AVAILABILITY STATEMENT

The original contributions presented in the study are included in the article/Supplementary Material, further inquiries can be directed to the corresponding author.

## AUTHOR CONTRIBUTIONS

All authors listed have made a substantial, direct, and intellectual contribution to the work and approved it for publication.

## FUNDING

This work is supported by the King Abdullah University of Science and Technology (KAUST), Saudi Arabia.

## ACKNOWLEDGMENTS

Authors would like to thank King Abdullah University of Science and Technology (KAUST), Saudi Arabia for the support.

## REFERENCES

Ahmad, I., Nguyen, K. D., and Letzepis, N. (2017). "Performance Analysis of High Throughput Satellite Systems with Optical Feeder Links," in IEEE Global Commun. Conf. (GLOBECOM), Singapore, 4–8 Dec 2017 (IEEE), 1–7. doi:10.1109/glocom.2017.8255105

Antonini, M., Betti, S., Carrozzo, V., Duca, E., and Ruggieri, M. (2006). "Feasibility Analysis of a HAP-LEO Optical Link for Data Relay Purposes," in IEEE Aero. Conf., Big Sky, MT, USA, 4–11 March 2006 (IEEE), 1–7.

Ashrafzadeh, B., Zaimbashi, A., Soleimani-Nasab, E., and Uysal, M. (2020). Unified Performance Analysis of Multi-Hop FSO Systems over Double Generalized Gamma Turbulence Channels with Pointing Errors. *IEEE Trans. Wireless Commun.* 19, 7732–7746. doi:10.1109/twc.2020.3015780

Beckmann, P., and Spizzichino, A. (1987). *The Scattering of Electromagnetic Waves from Rough Surfaces*. Norwood, MA, USA: Artech House Radar Library; Artech Print on Demand.

Bhatnagar, M. R., and Arti, M. K. (2013). Performance Analysis of Hybrid Satellite-Terrestrial FSO Cooperative System. *IEEE Photon. Technol. Lett.* 25, 2197–2200. doi:10.1109/lpt.2013.2282836

Chen, J., Yang, L., Wang, W., Yang, H.-C., Liu, Y., Hasna, M. O., et al. (2019). A Novel Energy Harvesting Scheme for Mixed FSO-RF Relaying Systems. *IEEE Trans. Veh. Technol.* 68, 8259–8263. doi:10.1109/tvt.2019.2925736

Datsikas, C. K., Peppas, K. P., Sagias, N. C., and Tombras, G. S. (2010). Serial Free-Space Optical Relaying Communications over Gamma-Gamma Atmospheric Turbulence Channels. *J. Opt. Commun. Netw.* 2, 576–586. doi:10.1364/jocn.2.000576

David, F., Giggenbach, D., Henniger, H., Horwath, J., Landrock, R., and Perlot, N. (2004). "Design Considerations for Optical Inter-HAP Links," in AIAA Int. Commun. Satellite Syst. Conf. Exhibit (ICSSC), 3144. doi:10.2514/6.2004-3144

d'Oliveira, F. A., Melo, F. C. L. D., and Devezas, T. C. (2016). High-Altitude Platforms—Present Situation and Technology Trends. *J. Aero. Technol. Manage.* 8, 249–262. doi:10.5028/jatm.v8i3.699

Farid, A. A., and Hranilovic, S. (2007). Outage Capacity Optimization for Free-Space Optical Links with Pointing Errors. *J. Lightwave Technol.* 25, 1702–1710. doi:10.1109/jlt.2007.899174

Fidler, F., Knapek, M., Horwath, J., and Leeb, W. R. (2010). Optical Communications for High-Altitude Platforms. *IEEE J. Select. Top. Quan. Electron.* 16, 1058–1070. doi:10.1109/jstqe.2010.2047382

Gao, N., Jin, S., Li, X., and Matthaiou, M. (2021). Aerial RIS-Assisted High Altitude Platform Communications. *IEEE Wireless Commun. Lett.* 10, 2096–2100. doi:10.1109/lwc.2021.3091164

Gradshteyn, I., and Ryzhik, I. (2000). *Table of Integrals, Series and Products*. 6th ed. New York, NY, USA: Academic.

ITU-Radiocommun (2000). *Preferred Characteristics of Systems in the Fixed Service Using High Altitude Platforms Operating in the Bands 47.2-47.5 GHz and 47.9-48.2 GHz*. Geneva: International Telecommunication Union, Electronic Publication. https://www.itu.int/dms_pubrec/itu-r/rec/f/R-REC-F.1500-0-200005-I!!PDF-E.pdf.

Jung, K.-J., Nam, S. S., Alouini, M.-S., and Ko, Y.-C. (2020). Unified Finite Series Approximation of FSO Performance Over Strong Turbulence Combined with Various Pointing Error Conditions. *IEEE Trans. Commun.* 68, 6413–6425. doi:10.1109/tcomm.2020.3008459

Kong, H., Lin, M., Zhu, W.-P., Amindavar, H., and Alouini, M.-S. (2020). Multiuser Scheduling for Asymmetric FSO/RF Links in Satellite-UAV-Terrestrial Networks. *IEEE Wireless Commun. Lett.* 9, 1235–1239. doi:10.1109/lwc.2020.2986750

Kurt, G. K., Khoshkholgh, M. G., Alfattani, S., Ibrahim, A., Darwish, T. S. J., Alam, M. S., et al. (2021). A Vision and Framework for the High Altitude Platform Station (HAPS) Networks of the Future. *IEEE Commun. Surv. Tutorials* 23, 729–779. doi:10.1109/comst.2021.3066905

Lee, J.-H., Park, K.-H., Ko, Y.-C., and Alouini, M.-S. (2020). Throughput Maximization of Mixed FSO/RF UAV-Aided Mobile Relaying with a Buffer. *IEEE Trans. Wireless Commun.* 20, 683–694. doi:10.1109/TWC.2020.3028068

Li, R., Chen, T., Fan, L., and Dang, A. (2019). Performance Analysis of a Multiuser Dual-Hop Amplify-And-Forward Relay System with FSO/RF Links. *J. Opt. Commun. Netw.* 11, 362–370. doi:10.1364/jocn.11.000362

Liu, X., Lin, M., Zhu, W.-P., Wang, J.-Y., and Upadhyay, P. K. (2020). Outage Performance for Mixed FSO-RF Transmission in Satellite-Aerial- Terrestrial Networks. *IEEE Photon. Technol. Lett.* 32, 1349–1352. doi:10.1109/lpt.2020.3025452

Michailidis, E. T., Nomikos, N., Bithas, P., Vouyioukas, D., and Kanatas, A. G. (2018). "Outage Probability of Triple-Hop Mixed RF/FSO/RF Stratospheric Communication Systems," in Proc. IEEE Int. Conf. Adv. Satellite Space Commun. (SPACOMM), Athens, Greece, April 22–26, 2018, 1–6.

Milas, V., Koletta, M., and Constantinou, P. (2003). Interference and Compatibility Studies Between Satellite Service Systems and Systems Using High Altitude Platform Stations. *ESA Spec. Publ.* 541, 34.

Miura, R., and Oodo, M. (2001). Wireless Communications System Using Stratospheric Platforms: R and D Program on Telecom and Broadcasting System Using High Altitude Platform Stations. *J. Commun. Res. Lab.* 48, 33–48.

Mozaffari, M., Saad, W., Bennis, M., Nam, Y.-H., and Debbah, M. (2019). A Tutorial on UAVs for Wireless Networks: Applications, Challenges, and Open Problems. *IEEE Commun. Surv. Tutorials* 21, 2334–2360. doi:10.1109/comst.2019.2902862

Parthasarathy, S., Giggenbach, D., and Kirstädter, A. (2014). "Channel Modelling for Free-Space Optical Inter-HAP Links Using Adaptive ARQ Transmission," in Unmanned/Unattended Sensors and Sensor Networks X (International Society for Optics and Photonics), Amsterdam, Netherlands, 17 October 2014, 9248, 92480Q. doi:10.1117/12.2067195

Saleh Altubaishi, E., and Alhamawi, K. (2019). Capacity Analysis of Hybrid AF Multi-Hop FSO/RF System Under Pointing Errors and Weather Effects. *IEEE Photon. Technol. Lett.* 31, 1304–1307. doi:10.1109/lpt.2019.2926679

Sharma, M., Chadha, D., and Chandra, V. (2016). High-Altitude Platform for Free-Space Optical Communication: Performance Evaluation and Reliability Analysis. *J. Opt. Commun. Netw.* 8, 600–609. doi:10.1364/jocn.8.000600

Sharma, S., Madhukumar, A. S., and R., S. (2019). Switching-Based Cooperative Decode-And-Forward Relaying for Hybrid FSO/RF Networks. *J. Opt. Commun. Netw.* 11, 267–281. doi:10.1364/jocn.11.000267

Shibata, Y., Kanazawa, N., Konishi, M., Hoshino, K., Ohta, Y., and Nagate, A. (2020). System Design of Gigabit HAPS Mobile Communications. *IEEE Access* 8, 157995–158007. doi:10.1109/access.2020.3019820

Singya, P. K., and Alouini, M.-S. (2021). Performance of UAV Assisted Multiuser Terrestrial-Satellite Communication System Over Mixed FSO/RF Channels. *IEEE Trans. Aero. Electron. Syst.* doi:10.1109/taes.2021.3111787

Singya, P. K., Kumar, N., Bhatia, V., and Alouini, M.-S. (2019). On Performance of Hexagonal, Cross, and Rectangular QAM for Multi-Relay Systems. *IEEE Access* 7, 60602–60616. doi:10.1109/access.2019.2915375

Singya, P. K., Kumar, N., Bhatia, V., and Alouini, M.-S. (2020). On the Performance Analysis of Higher Order QAM Schemes Over Mixed RF/FSO Systems. *IEEE Trans. Veh. Technol.* 69, 7366–7378. doi:10.1109/tvt.2020.2990747

Singya, P. K., Kumar, N., and Bhatia, V. (2018). Impact of Imperfect CSI on ASER of Hexagonal and Rectangular QAM for AF Relaying Network. *IEEE Commun. Lett.* 22, 428–431. doi:10.1109/lcomm.2017.2778153

Swaminathan, R., Sharma, S., Vishwakarma, N., and Madhukumar, A. (2021). HAPS-Based Relaying for Integrated Space-Air-Ground Networks with Hybrid FSO/RF Communication: A Performance Analysis. *IEEE Trans. Aero. Electron. Syst.* 57, 1581–1599. doi:10.1109/TAES.2021.3050663

Trichili, A., Cox, M. A., Ooi, B. S., and Alouini, M.-S. (2020). Roadmap to Free Space Optics. *J. Opt. Soc. Am. B* 37, A184–A201. doi:10.1364/josab.399168

Trichili, A., Ragheb, A., Briantcev, D., Esmail, M. A., Altamimi, M., Ashry, I., et al. (2021). Retrofitting FSO Systems in Existing RF Infrastructure: A Non-Zero-Sum Game Technology. *IEEE Open J. Commun. Soc.* 2, 2597–2615. doi:10.1109/ojcoms.2021.3130645

Vaiopoulos, N., Sandalidis, H. G., and Varoutas, D. (2013). Using a HAP Network to Transfer WiMAX OFDM Signals: Outage Probability Analysis. *J. Opt. Commun. Netw.* 5, 711–721. doi:10.1364/jocn.5.000711

Wang, P., Cao, T., Guo, L., Wang, R., and Yang, Y. (2015). Performance Analysis of Multihop Parallel Free-Space Optical Systems Over Exponentiated Weibull Fading Channels. *IEEE Photon. J.* 7, 1–17. doi:10.1109/jphot.2015.2396115

Wolframe (1998). The Wolfram Function Site. Available at: http://functions.wolfram.com/.

Xu, G., and Song, Z. (2020). Performance Analysis for Mixed $\kappa$-$\mu$ Fading and M-Distribution Dual-Hop Radio Frequency/Free Space Optical Communication Systems. *IEEE Trans. Wireless Commun.* 20, 1517–1528. doi:10.1109/TWC.2020.3034104

Xu, G., and Song, Z. (2021). Performance Analysis of a UAV-Assisted RF/FSO Relaying Systems for Internet of Vehicles. *IEEE Internet Things J.* doi:10.1109/JIOT.2021.3051211

Xu, G., and Zhang, Q. (2021). Mixed RF/FSO Deep Space Communication System Under Solar Scintillation Effect. *IEEE Trans. Aero. Electron. Syst.* 57, 3237–3251. doi:10.1109/taes.2021.3074130

Yang, L., Yuan, J., Liu, X., and Hasna, M. O. (2018). On the Performance of LAP-Based Multiple-Hop RF/FSO Systems. *IEEE Trans. Aero. Electron. Syst.* 55, 499–505. doi:10.1109/TAES.2018.2852399

Zedini, E., and Alouini, M.-S. (2015). Multihop Relaying over IM/DD FSO Systems with Pointing Errors. *J. Lightwave Technol.* 33, 5007–5015. doi:10.1109/jlt.2015.2492244

Zedini, E., Kammoun, A., and Alouini, M.-S. (2020). Performance of Multibeam Very High Throughput Satellite Systems Based on FSO Feeder Links with HPA Nonlinearity. *IEEE Trans. Wireless Commun.* 19, 5908–5923. doi:10.1109/twc.2020.2998139

Zedini, E., Soury, H., and Alouini, M.-S. (2016). On the Performance Analysis of Dual-Hop Mixed FSO/RF Systems. *IEEE Trans. Wireless Commun.* 15, 3679–3689. doi:10.1109/twc.2016.2524685

Zhan, P., Yu, K., and Swindlehurst, A. L. (2011). Wireless Relay Communications with Unmanned Aerial Vehicles: Performance and Optimization. *IEEE Trans. Aerosp. Electron. Syst.* 47, 2068–2085. doi:10.1109/taes.2011.5937283

**Conflict of Interest:** The authors declare that the research was conducted in the absence of any commercial or financial relationships that could be construed as a potential conflict of interest.

**Publisher's Note:** All claims expressed in this article are solely those of the authors and do not necessarily represent those of their affiliated organizations, or those of the publisher, the editors and the reviewers. Any product that may be evaluated in this article, or claim that may be made by its manufacturer, is not guaranteed or endorsed by the publisher.

## APPENDIX

We have considered the Gamma-Gamma distribution for the atmospheric turbulence modeling of the ES-HAP FSO link and Meijer-G function is the prime element in the analytical expression. Hence, for asymptotic analysis, the meijer-G function must be approximated at high SNR which can be represented by the basic elementary form as (Wolframe, 1998, (07.34.06.0001.01))

$$\mathrm{G}_{c,d}^{a,b}\left[x\middle|\begin{matrix}\varrho_3\\ \varrho_4\end{matrix}\right] \approx \sum_{p=1}^{a} x^{\varrho_{4,p}} \frac{\prod_{\substack{q=1\\ q\neq p}}^{a}\Gamma\left(\varrho_{4,q}-\varrho_{4,p}\right)\prod_{q=1}^{b}\Gamma\left(1-\varrho_{3,q}+\varrho_{4,p}\right)}{\prod_{q=b+1}^{c}\Gamma\left(\varrho_{3,q}-\varrho_{4,p}\right)\prod_{a+1}^{d}\Gamma\left(1-\varrho_{4,q}+\varrho_{4,p}\right)}, \tag{34}$$

where $\varrho_3 = [1, \varrho_1]$ and $\varrho_4 = [\varrho_2, 0]$. As the power on the transmit SNR term decides the diversity order, the dominant term from **(34)** can be obtained as $\min\left(\frac{e^2}{r}, \frac{\alpha}{r}, \frac{\beta}{r}\right)$. Now considering the high SNR approximation of $\Upsilon(m,x) \underset{x\to 0}{\approx} \frac{x^m}{m}$, the CDF and PDF of the Nakagami-m distributed RF link for the $u$th MU can be approximated as $f_{\gamma_{HM_u}}(x) \approx \frac{1}{\Gamma(mN_t)}\left(\frac{m}{\bar{\gamma}_U}\right)^{mN_t} x^{mN_t-1}$ and $F_{\gamma_{HM_u}}1850\%(x) \approx \frac{1}{\Gamma(mN_t)}\left(\frac{m}{\bar{\gamma}_U}x\right)^{mN_t}$, respectively. Substituting the approximate CDF and PDF expression in **(23)**, the CDF expression of HAP-MU terrestrial link can be approximated as

$$F_{\gamma_{HM}}^{A}(\gamma_{th}) \approx \left(\frac{1}{\Gamma(mN_t+1)}\right)^{U}\left(\frac{m\gamma_{th}}{\bar{\gamma}_U}\right)^{UmN_t}. \tag{35}$$

From **(35)**, it is observed that the diversity order of the RF link is $U \times m \times N_t$ which directly depends on the number of terrestrial MUs ($U$), number of antennas ($N_t$), and RF link's fading severity $m$. Finally, substituting (**34**) and (**35**) in **(29)**, asymptotic outage probability for the considered system is obtained as (**30**).